European Radiology (2019) 29:5539–5548
https://doi.org/10.1007/s00330-019-06097-9

NEURO

Permeability measurement using dynamic susceptibility contrast magnetic resonance imaging enhances differential diagnosis of primary central nervous system lymphoma from glioblastoma

Ji Ye Lee[1] · Atle Bjørnerud[2,3] · Ji Eun Park[4] · Bo Eun Lee[5] · Joo Hyun Kim[6] · Ho Sung Kim[4]

Received: 28 August 2018 / Revised: 10 January 2019 / Accepted: 11 February 2019 / Published online: 15 March 2019

Abstract

Objectives To test if adding permeability measurement to perfusion obtained from dynamic susceptibility contrast MRI (DSC-MRI) improves diagnostic performance in the differentiation of primary central nervous system lymphoma (PCNSL) from glioblastoma.

Materials and methods DSC-MRI was acquired in 145 patients with pathologically proven glioblastoma ($n = 89$) or PCNSL ($n = 56$). The permeability metrics of contrast agent extraction fraction (E_x), apparent permeability (K_a), and leakage-corrected perfusion of normalized cerebral blood volume ($nCBV_{res}$) and cerebral blood flow ($nCBF_{res}$) were derived from a tissue residue function. For comparison purposes, the leakage-corrected normalized CBV (nCBV) and relative permeability constant (K_2) were also obtained using the established Weisskoff-Boxerman leakage correction method. The area under the receiver operating characteristics curve (AUC) and cross-validation were used to compare the diagnostic performance of the single DSC-MRI parameters with the performance obtained with the addition of permeability metrics.

Results PCNSL demonstrated significantly higher permeability (E_x, $p < .001$) and lower perfusion ($nCBV_{res}$, $nCBF_{res}$, and nCBV, all $p < .001$) than glioblastoma. The combination of E_x and $nCBV_{res}$ showed the highest performance (AUC, 0.96; 95% confidence interval, 0.92–0.99) for differentiating PCNSL from glioblastoma, which was a significant improvement over the single perfusion (nCBV: AUC, 0.84; $nCBV_{res}$: AUC, 0.84; $nCBF_{res}$: AUC, 0.82; all $p < .001$) or E_x (AUC, 0.80; $p < .001$) parameters.

Conclusions Analysis of the combined permeability and perfusion metrics obtained from a single DSC-MRI acquisition improves the diagnostic value for differentiating PCNSL from glioblastoma in comparison with single-parameter nCBV analysis.

Key Points

- *Permeability measurement can be calculated from DSC-MRI with a tissue residue function-based leakage correction.*
- *Adding E_x to CBV aids in the differentiation of PCNSL from glioblastoma.*
- *CBV and E_x measurements from DSC-MRI were highly reproducible.*

Keywords Glioblastoma · Lymphoma · Perfusion magnetic resonance imaging · Magnetic resonance imaging · Permeability

Ji Ye Lee and Atle Bjørnerud contributed equally to this work.

Electronic supplementary material The online version of this article (https://doi.org/10.1007/s00330-019-06097-9) contains supplementary material, which is available to authorized users.

✉ Ji Eun Park
jieunp@gmail.com

[1] Department of Radiology, Eulji Medical Center, Seoul 01830, Republic of Korea

[2] Department of Diagnostic Physics, Division of Radiology and Nuclear Medicine, Oslo University Hospital, Oslo, Norway

[3] Department of Physics, University of Oslo, Oslo, Norway

[4] Department of Radiology and Research Institute of Radiology, Asan Medical Center, University of Ulsan College of Medicine, 43 Olympic-ro 88, Songpa-Gu, Seoul 05505, Republic of Korea

[5] Department of Radiology, Boramae Medical Center, Seoul Metropolitan Government -Seoul National University, Seoul, Republic of Korea

[6] NordicNeuroLab, LLC, Seoul, Republic of Korea

Abbreviations

AUC	Area under the receiver operating characteristics curve
DCE	Dynamic contrast-enhanced
DSC	Dynamic susceptibility contrast
E_x	Extraction fraction
K_2	Relative permeability constant
K_a	Apparent permeability
K^{trans}	Contrast agent transfer constant
$nCBF_{res}$	Leakage-corrected normalized cerebral blood flow from a tissue residue function-based method
nCBV	Normalized cerebral blood volume from a Weisskoff-Boxerman method
$nCBV_{res}$	Leakage-corrected normalized cerebral blood volume from a tissue residue function-based method

Introduction

Microvascular permeability and angiogenesis can be measured noninvasively with T1-based dynamic contrast-enhanced (DCE) MRI and T2*-based dynamic susceptibility contrast (DSC) MRI [1]. Primary central nervous system lymphoma (PCNSL) is characterized by less neovascularization than glioblastoma [2], and perfusion MRI techniques can aid in the differential diagnosis. DSC-MRI is the most established method for differential diagnosis, and several studies show reduced cerebral blood volume (CBV) in PCNSL compared with glioblastoma [3, 4], findings that were further confirmed by a meta-analysis [5]. However, the results for agent permeability measurements derived from DCE-MRI, are less clear-cut. Although some studies show increased permeability (in terms of the contrast agent transfer constant K^{trans}) in PCNSL compared with glioblastoma [6], others have not found significant differences in K^{trans} between the two tumor types [7]. Furthermore, the analysis of permeability from DCE-MRI as an addition to DSC-MRI normally requires an additional contrast agent injection, which adds to the scan time and complexity of the examination [8].

In DSC-MRI, contrast agent extravasation is usually considered to be a confounding effect, in that it may lead to either over- or under-estimation of CBV, depending on the dominant contrast mechanism of gadolinium (T1 or T2* effect) in the leakage space [9, 10]. To this end, several CBV leakage correction methods have been proposed, with the Weisskoff-Boxerman method, which estimates leakage from the deviation in each voxel from a leakage-independent reference tissue response curve, being the most established approach [11]. However, a potential limitation of this method is its sensitivity to variations in mean transit time (MTT) relative to the reference curve MTT, as deviations from the reference MTT may be interpreted as leakage effects [9]. Bjørnerud et al recently proposed an alternative approach, whereby perfusion and permeability metrics are derived directly from the tissue residue function obtained by deconvolution with an automatically generated arterial input function (AIF) [9]. In addition to providing MTT insensitive leakage-corrected CBV and CBF estimates, this approach also provides estimates of contrast agent permeability and extraction fraction (E_x), potentially adding diagnostic value beyond the standard DSC-MRI-based perfusion analysis. However, the theoretical differences have not been demonstrated in a clinical study.

To this end, the primary aim of the present work was to test whether additional permeability-related parameters obtained from the tissue residue function approach can improve the differentiation of PCNSLs from glioblastomas in comparison with conventional DSC-MRI analysis. A secondary aim was to compare perfusion metrics obtained from two different leakage correction methods in terms of their diagnostic accuracy in the differentiation of PCNSL from glioblastoma.

Material and methods

Patients

Our institutional review board approved this retrospective study and the requirement for informed consent was waived. The electronic database of the Department of Radiology was searched, and patient records for the period January 2013 to June 2017 were retrospectively reviewed. One hundred fifty-nine consecutive patients with pathologically confirmed glioblastoma ($n = 98$) or PCNSL ($n = 61$) according to the 2016 WHO Classification of Tumors of the CNS [12] were identified. All patients underwent MRI including contrast-enhanced T1-weighted imaging (CE-T1WI), FLAIR, DWI, and DSC-MRI. Patients were excluded if they had a prior history of corticosteroid ($n = 2$) or other treatment ($n = 1$), or DSC-MRI data were missing ($n = 5$) or unreadable ($n = 6$, because of an artifact). These steps yielded 145 patients (mean age, 53.3 years; range, 28–86 years; male: female ratio, 75:70) with glioblastoma ($n = 89$) or PCNSL ($n = 56$).

MRI protocol

All MRI studies were performed using a 3-T MR system (Achieva; Philips Medical Systems,) with an 8-channel sensitivity encoding head coil. The dedicated MR protocol for brain tumors at our institution consisted of T2-weighted imaging, FLAIR, T1-weighted imaging, DWI, DSC-MRI, and CE-T1WI.

DSC-MRI was acquired using a gradient-echo echo-planar imaging protocol. A preload of 0.01 mmol/kg gadoterate meglumine was given before the dynamic bolus, then the dynamic bolus was administered as a standard dose of 0.1 mmol/kg gadoterate meglumine (Dotarem; Guerbet) delivered at a rate of

4 mL/s by a MRI-compatible power injector (Spectris; Medrad). The bolus of contrast material was followed by a 20 mL bolus of saline, injected at the same rate. The parameters for the DSC-MRI included the following: repetition time (TR)/echo time (TE), 1808/40 ms; flip angle, 35°; field of view, 24 × 24 cm; slice thickness/gap, 5/2 mm; matrix, 128 × 128; total acquisition time, 1 min and 54 s. The dynamic acquisition was performed with a temporal resolution of 1.5 s, and 60 dynamics were acquired. DSC-MRI was acquired with complete tumor volume coverage and the same section orientations as used in the conventional MRI. We used both predosing and mathematical post-processing methods for DSC-MRI images to reduce extravasation-induced errors in the CBV estimates [10].

Image post-processing

DSC-MRI data were transferred to an independent workstation and processed using nordicICE (V.4.0.6; NordicNeuroLab AS) software.

Two post-processing methods for leakage correction were compared, the residue function-based contrast leakage correction method [9, 13] and the method of Weisskoff and Boxerman et al [11, 14].

The tissue residue function-based leakage correction method fits the tissue residue function to a two-compartment uptake kinetic model. The tissue response to a given AIF is described by the convolution integral:

$$\Delta R2^{*}{}_{\text{tissue}}(t) = F \cdot \Delta R2^{*}{}_{\text{AIF}}(t) \otimes H(t) \quad (1)$$

where $\Delta R2^{*}{}_{\text{tissue}}(t)$ and $\Delta R2^{*}{}_{\text{AIF}}(t)$ are the measured changes in the transverse relaxation rate in tissue and the feeding artery (AIF), F is fractional tissue perfusion, and $\otimes$ is the convolution operator. The two-compartment uptake model explains continuous extravasation along the capillaries, but reflux of the contrast agent from the extracellular extravascular space (EES) to the plasma space (PS) is assumed negligible during the observation duration [15]. $H(t)$ is the residue function describing the probability of contrast agent being present in a tissue at a given time t following an instantaneous bolus injection of contrast agent. $R(t)$ is the product of $F \cdot H(t)$ and can be calculated using standard deconvolution technique, and F is then estimated from the peak height of the $R(t)$. Assuming the two-compartment uptake model to be a valid approximation, the residue function can be approximated by the following function:

$$H(t) = \exp\left(-\frac{t}{T_{\text{p}}}\right) + E_{\text{x}}\left[1-\exp\left(-\frac{t}{T_{\text{p}}}\right)\right] \quad (2)$$

where E_{x} is the extraction fraction that describes the fraction of contrast agent extracted during the first pass through tissue and T_{p} is the plasma MTT. Then, $H(t)$ obtained by deconvolution was fitted to Eq. 2 using a non-linear least squares algorithm, giving E_{x} and T_{p}. The term $\exp\left(-\frac{t}{T_{\text{p}}}\right)$ represents the perfusion phase, and $E_{\text{x}}\left[1-\exp\left(-\frac{t}{T_{\text{p}}}\right)\right]$ represents the extravasation phase, as shown schematically in Fig. 1.

The transfer constant, K^{trans}, is then given by

$$K^{\text{trans}} = E_{\text{x}} \cdot \text{F} \quad (3)$$

From Eq. 1, the perfusion (in units of mL of blood/100 g per min) is given by:

$$CBF_{\text{res}} = \varsigma \cdot F \quad (4)$$

where ς is a scaling factor (including tissue density and time unit conversion). F is fractional tissue perfusion calculated from deconvolution with singular value decomposition [16].

The capillary MTT (MTT_{res}) is derived from the time constant T_{p} as follows:

$$\text{MTT}_{\text{res}} = \frac{T_{\text{p}}}{1-E_{\text{x}}} \quad (5)$$

The tissue volume fraction is then calculated from the central volume theorem:

$$\text{CBV}_{\text{res}} = \varsigma \cdot F \cdot \text{MTT}_{\text{ref}} \quad (6)$$

The Weisskoff-Boxerman method is based on time-dependent deviation of the pixel-wise concentration time curve from a reference curve assumed to be unaffected by leakage [11]. The details of the Weisskoff-Boxerman method are shown in the Supplementary Materials.

For both correction methods, the raw time-intensity curve was initially converted to $\Delta R2^{*}(t)$, assuming a mono-exponential relationship between the MR signal and contrast agent-induced change in $R2^{*}$. The residue-based method requires additional estimation of the AIF, which was automatically obtained as previously proposed [9, 13]. To better compare the metrics obtained with the different correction methods, CBV and CBF values were automatically normalized (nCBV, nCBF) to the corresponding mean parameter value in apparently unaffected brain tissue, as previously described [17]. Using the same terminology as in [9], the transfer constant estimated from the residue method is referred to as K_{a}, reflecting the fact that it is an apparent transfer constant due to possible confounding mixes of T1 and T2* relaxation effects. K_{a} and K_2 were not normalized since their values in the unaffected brain are close to zero.

Image analysis

The quantitative maps (nCBV_{res}, nCBF_{res}, MTT_{res}, K_{a}, and E_{x} from the tissue residue function-based method, and nCBV and

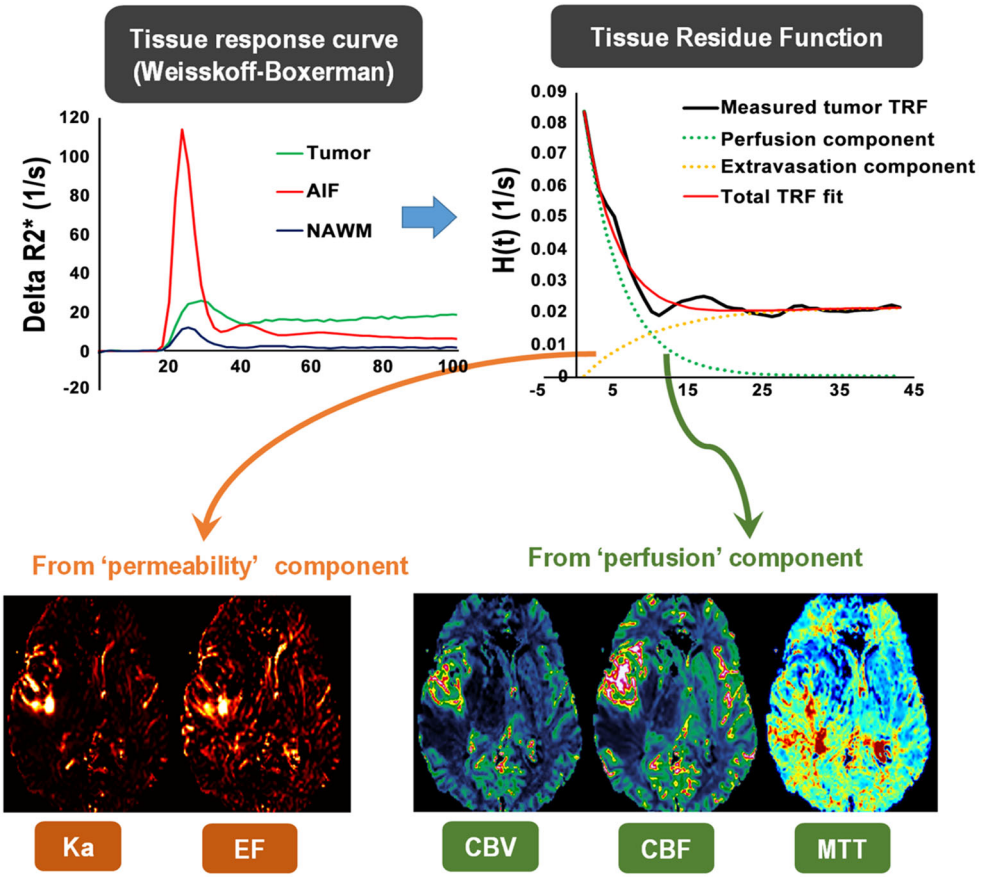

Fig. 1 Workflow of the combined permeability/perfusion analysis using the tissue residue function (TRF) approach. The pixel-wise TRF is obtained by deconvolution of the (automatically determined) arterial input function (AIF) with the tissue response curves. The resulting TRF is then fitted to the two-compartment uptake model, providing estimates of a "perfusion" and a "permeability" components, respectively, resulting in the output of both permeability-related (contrast agent transfer constant, K_a, and extraction fraction, E_x) and perfusion-related (cerebral blood volume, CBV, cerebral blood flow, CBF and mean transit time, MTT) parametric maps

K_2 from the Weisskoff-Boxerman method) were generated and co-registered to the CE-T1WI images before all imaging analysis. A volume-of-interest (VOI) was drawn slice by slice on the CE-T1WI images using the semi-automated segmentation method available within the software (nordicICE). The VOI was drawn by an experienced radiologist (J.Y.L., with 4 years of experience in neuroradiology), who were blinded to the histopathologic data, to include all contrast-enhancing areas, excluding areas of necrosis or non-tumor macro-vessels. The value of each DSC parameter was then estimated for the whole VOI by summing up all values from each axial slice and averaging them. The tumor volume was automatically calculated based on VOI.

The reproducibility of the DSC parameters was assessed by repeating the measurements on 20 patients (10 patients from each group) using VOIs drawn by another neuroradiologist (B.E.L. with 3 years of experience).

Statistical analysis

All continuous variables were assessed for normality using the Kolmogorov-Smirnov test. Values are expressed as mean ± standard deviation (SD) for continuous variables. The clinical characteristics of patients with PCNSLs and glioblastomas were compared using the χ^2 test for categorical variables and Student's t test for continuous variables, after normality and equivalent variance testing. Student's t test was used to compare the DSC parameters between the two groups. We performed multivariate logistic regression analysis to find a significant predictor to diagnose between PCNSL and glioblastoma.

The diagnostic performance for differentiating glioblastoma from PCNSL was assessed by area under the receiver operating characteristics curve (AUC) analysis. Optimal threshold for the DSC parameters was determined by the Youden index, by maximizing the total of the sensitivity and specificity values to differentiate between PCNSL and glioblastoma [18]. The main goal was to measure the maximum potential effectiveness of the biomarkers of interest (CBV, E_x, CBF in our study) for differentiating PCNSL from glioblastoma. The threshold giving maximum Youden index is referred to as the optimal cut-off point because this threshold value yields maximal ability of the biomarkers to differentiate glioblastoma from PCNSL. For further validation, bootstrap resampling (1000 iterations) and leave-one-out cross-validation were used. In this method, all patients except one were used as the training set, and the prediction error

was assessed for the excluded validation set. This procedure was repeated until every case was used once as a validation set. The confidence intervals (CIs) for diagnostic accuracy, sensitivity, specificity, positive predictive value, and negative predictive value were calculated using this method.

Additionally, correlations between perfusion parameters across all patients were calculated.

To test reproducibility, inter-observer agreement between the two readers was calculated using the intraclass correlation coefficient (ICC). The "pROC" and "cvTools" packages in R version 3.3.3 (R Project for Statistical Computing, http://www.r-project.org) were used for the comparisons of AUCs and cross-validation. For all statistical comparisons, p values < .05 were accepted as indicating a significant statistical difference. Bonferroni correction was applied to adjust the p values for multiple comparisons, with a Bonferroni-corrected significance level of $p < .007$ being used for comparing DSC-MRI parameters between PCNSL and glioblastomas, and $p < .0125$ for comparing the diagnostic performance of the combined model with that of the single DSC parameters.

Results

The clinical characteristics of the study patients are summarized in Table 1. There were no significant differences in patient sex, age, or tumor volume between the two groups. All patients had diffuse large B cell lymphoma in the PCNSL group. In glioblastoma, 78 patients were IDH (isocitrate dehydrogenase)-wild type and 9 patients were IDH-mutated type.

Comparison of DSC-MRI parameters between PCNSL and glioblastoma

Table 2 summarizes the comparison of the DSC-MRI parameters between PCNSL and glioblastoma. PCNSLs showed significantly lower perfusion than glioblastomas on $nCBV_{res}$ (mean ± SD, PCNSL: 1.82 ± 0.96 vs. glioblastoma: 3.15 ± 1.20 relative units, $p < .001$), $nCBF_{res}$ (1.39 ± 0.65 vs. 2.41 ± 1.33 relative units, $p < .001$), and nCBV (1.48 ± 0.61 vs. 2.67 ± 1.24 relative units, $p < .001$) parameter maps. There was no significant difference in MTT_{res} or the contrast agent transfer constant using either method (K_2 or K_a).

PCNSL demonstrated significantly higher E_x (11.0% ± 6.75%) than glioblastoma (5.30% ± 2.62%, $p < .001$).

Figures 2 and 3 show example cases of DSC parameters from PCNSL and glioblastoma.

The diagnostic value of adding E_x to perfusion parameters in the differentiation of PCNSL from glioblastoma

Results of univariate and multivariate analyses are shown in Table 3. For the multivariate analysis, lower $nCBV_{res}$ and higher E_x were independent predictors to distinguish PCNSL from glioblastoma. The overall model fit (df = 4) was $\chi^2 = 106.3$ ($p < .001$), with Nagelkerke $R^2 = 0.7054$. The diagnostic performances of the different parameter combinations for the differentiation of PCNSL from glioblastoma are shown in Table 4. Among the single DSC parameters, $nCBV_{res}$ (AUC, 0.84; 95% CI, 0.77–0.90) and nCBV (AUC, 0.84; 0.77–0.90) exhibited a similar high diagnostic performance for differentiating PCNSL from glioblastoma, followed by $nCBF_{res}$ (AUC, 0.82; 0.74–0.88) and E_x (AUC, 0.80; 0.73–0.86).

Table 1 Clinical characteristics of the study patients

	PCNSL	Glioblastoma	p value
Number of patients	56	89	
Number of male patients (%)	27 (48)	48 (54)	.54
Age	58.6 ± 7.3	55.2 ± 8.1	.34
Tumor volume (mL)	11.1 ± 9.8	13.3 ± 11.5	.20
Histopathology	Diffuse large B cell lymphoma	Glioblastoma	
IDH mutation status (No.)	NA	Mutated (9)	
		Wild type (78)	
		NA (2)	

Data are expressed as mean ± standard deviation for continuous variables. *PCNSL*, primary central nervous system lymphoma; *IDH*, isocitrate dehydrogenase 1 mutation

A combination of perfusion and permeability metrics was feasible with the tissue residue function-based method, and the two best performers, E_x and $nCBV_{res}$, were selected. The combination of E_x and $nCBV_{res}$ exhibited a high diagnostic performance (AUC, 0.96; 0.92–0.99) for differentiation of PCNSL from glioblastoma, with a sensitivity of 94.6%, a specificity of 97.8%, and an accuracy of 96.6%. The diagnostic performance was significantly improved in comparison with any single perfusion or permeability parameter (nCBV, nCBF, CBF_{res}, and E_x; all $p < .001$, Bonferroni-corrected) (Fig. 4). The bootstrapped leave-one-out cross-validation demonstrated the same trend of improved performance when using a combination of perfusion and permeability parameters in comparison with any single parameter.

The sensitivities, specificities, and positive/negative predictive values of metrics are summarized in Supplementary Table 1.

$nCBV_{res}$ and E_x showed a mild negative correlation ($r = -0.29$, $p < .001$). nCBV and $nCBV_{res}$ showed a strong positive correlation ($r = 0.91$, $p < .001$).

Reproducibility of DSC measurements

Inter-observer agreement for quantitative measures of the DSC parameters between the two readers was almost perfect (ICC, 0.98–0.99; 95% CI, 0.98–0.99).

Table 2 Comparison of dynamic susceptibility contrast MRI parameters between primary central nervous system lymphomas and glioblastomas

Processing method	PCNSL	Glioblastoma	*p* value
Tissue residue function-based			
$nCBV_{res}$ (relative units)	1.82 ± 0.96	3.15 ± 1.20	<.001*
MTT_{res} (s)	7.49 ± 2.67	8.28 ± 2.30	.06
$nCBF_{res}$ (relative units)	1.39 ± 0.65	2.41 ± 1.33	<.001*
K_a	0.14 ± 0.11	0.15 ± 0.20	.50
E_x (%)	11.0 ± 6.75	5.30 ± 2.62	<.001*
Weisskoff-Boxerman			
nCBV (relative units)	1.48 ± 0.61	2.67 ± 1.24	<.001*
K_2	0.90 ± 0.81	1.25 ± 1.14	.05

CBV, cerebral blood volume; *nCBV*, leakage-corrected normalized CBV derived using the reference method; *nCBF*, leakage-corrected normalized cerebral blood flow derived using the reference method; $nCBV_{res}$, leakage-corrected normalized CBV derived using the tissue residue function-based method; MTT_{res}, mean transit time derived using the tissue residue function-based method; $nCBF_{res}$, leakage-corrected normalized CBF derived using the tissue residue function-based method; K_2, leakage parameter accounting for T2* leakage effect; K_a, apparent transfer constant; E_x, extraction fraction. *Significant *p* value after Bonferroni correction ($p < 0.001$)

Discussion

In this study, we tested the clinical utility of permeability and perfusion metrics in the differentiation of PCNSL from glioblastoma, with all metrics being simultaneously estimated from a single DSC-MRI acquisition. The main finding was that the contrast agent extraction fraction, E_x, which was estimated from the tissue residue function, was significantly higher in PCNSL than in glioblastoma, while both relative perfusion and blood volume were significantly lower in PCNSL than in glioblastoma. This opposite trends of permeability and perfusion suggest a favorable combined effect on diagnostic performance. A combined model of E_x and $nCBV_{res}$ yielded the highest diagnostic performance and higher than any single DSC parameter to differentiate PCNSL from glioblastoma. This finding is supported by multivariate logistic regression analysis that only E_x and $nCBV_{res}$ were independent predictors to the differential diagnosis.

Our study shows the complementary information obtained from permeability analysis potentially enhancing the diagnostic performance of DSC-MRI in brain tumors. Such combined analyses yielded higher sensitivity and specificity compared to any single perfusion or permeability metric and may aid in clinical decision-making by increasing the confidence in PCNSL diagnosis and hence reduce putative surgical removal.

In comparison with glioblastoma, PCNSLs exhibit poor neovascularization and angiocentric tumor growth [19, 20]. While it is well established that CBV obtained from DSC-MRI is lower in PCNSL than in glioblastoma, it is not so clear-cut whether there is a corresponding difference in permeability (K^{trans}) obtained from DCE-MRI. Although several studies suggest that permeability is higher in PCNSL than in glioblastoma, others have not been able to detect any difference between the two tumor types [17]. In the present study, we found no significant difference in apparent permeability (K_a) between PCNSL and glioblastoma. The significantly higher E_x in PCNSL can therefore be explained by the lower nCBF in these tumors, without a corresponding reduction in permeability, as $E_x = K_a/CBF$.

Other approaches have been proposed for obtaining combined perfusion and permeability data from contrast-enhanced MRI. Combined perfusion and permeability analysis was previously shown to be feasible using DCE-MRI with a high temporal resolution [21]. Further, the use of a dual injection approach has also been reported whereby a DCE-MRI acquisition is immediately followed by a DSC-MRI using separate contrast injections [22]. Although this latter approach requires a double-contrast injection and increased overall scan time, it allows optimal protocols for both DCE and DSC analysis. Further, through the initial DCE-contrast injection, this approach provides the necessary pre-bolus condition for minimizing T1-dominant leakage effects in the DSC-MRI acquisition. DCE-MRI also has advantages over DSC-MRI in that

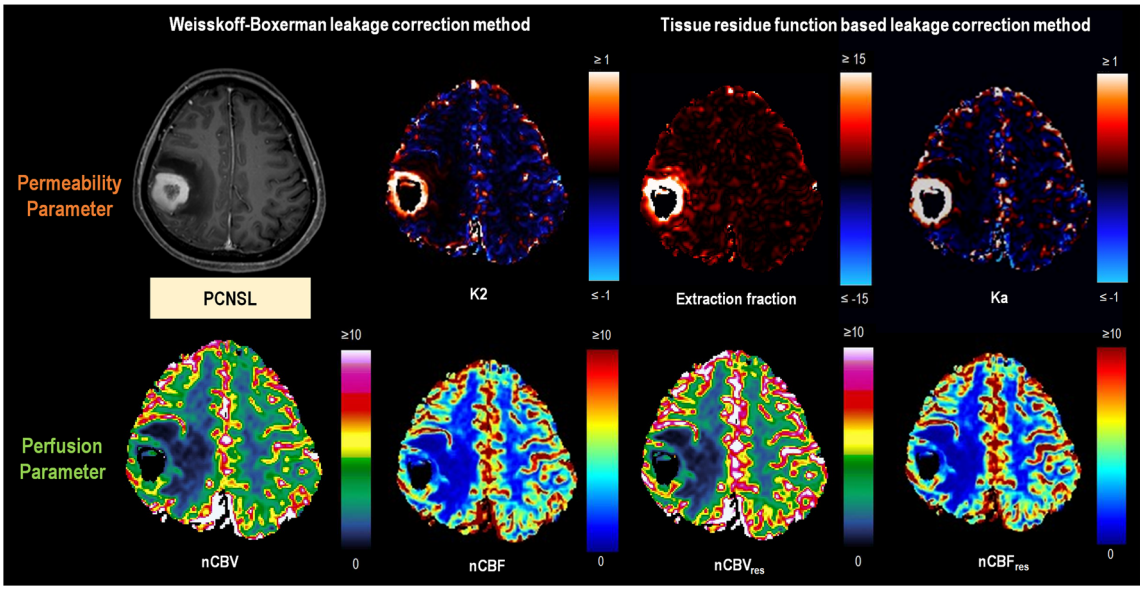

Fig. 2 A 62-year-old female patient with primary central nervous system lymphoma (PCNSL). The PCNSL shows minimally increased perfusion parameters of cerebral blood volume (CBV) and cerebral blood flow (CBF), and markedly increased permeability including leakage parameter accounting for T2* leakage effect (K_2), apparent transfer constant (K_a), and extraction fraction (E_x). Note that the elevation of E_x is mostly pronounced within the enhancing portion of the tumor

it is less sensitive to susceptibility artifacts and may provide a more predictable dose response [21].

However, DSC-MRI-based methods do have advantages over DCE-MRI in terms of the higher temporal resolution (enabling full brain coverage) and significantly higher contrast agent sensitivity [23]. DSC-MRI-based analysis of permeability-related metrics has showed robustness, both theoretically and practically, in permeability measurement with DSC-MRI. Both T1 and T2* relaxation effects in the extracellular extravascular space can be separately calculated with both positive and negative apparent rate constants [9] and gives robust estimation of contrast agent extravasation. Using clinical data, the method also exhibited high test-retest stability investigated in 28 recurrent glioma patients [13]. Based on the favorable properties of DSC-MRI and previous results combining perfusion and permeability modeling, we

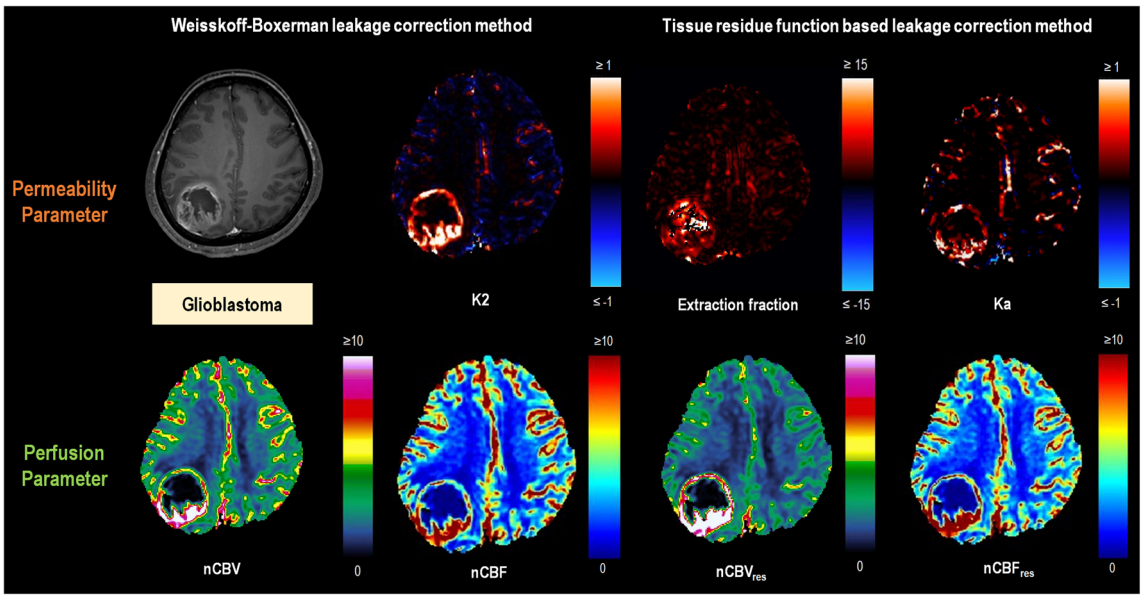

Fig. 3 A 58-year-old female patient with glioblastoma. The glioblastoma shows increased perfusion parameters of cerebral blood volume (CBV) and cerebral blood flow (CBF), and increased permeability including leakage parameter accounting for T2* leakage effect (K_2), apparent transfer constant (K_a), and extraction fraction (E_x). Note that the elevation of E_x and K_a is less pronounced than K_2, which is a by-product of a tissue response curve from the Weisskoff-Boxerman method

Table 3 Uni- and multivariate analysis of imaging parameters to distinguish PCNSL from glioblastoma

Variables	Univariate		Multivariate	
	Odds ratio (95% CI)	*p* value	Odds ratio (95% CI)	*p* value
Tissue residue function-based				
$nCBV_{res}$	0.26 (0.16, 0.43)	< .001	0.36 (0.21, 0.63)	< .001
MTT_{res}	0.87 (0.75, 1.01)	0.066		
$nCBF_{res}$	0.21 (0.11, 0.41)	< .001		
K_a	0.45 (0.04, 4.89)	0.510		
E_x	1.41 (1.24, 1.60)	< .001	1.50 (1.27–1.77)	< .001
Weisskoff-Boxerman				
nCBV	0.17 (0.09, 0.33)	< .001		
K_2	0.61 (0.37, 0.98)	0.04	0.49 (0.22, 1.13)	0.09

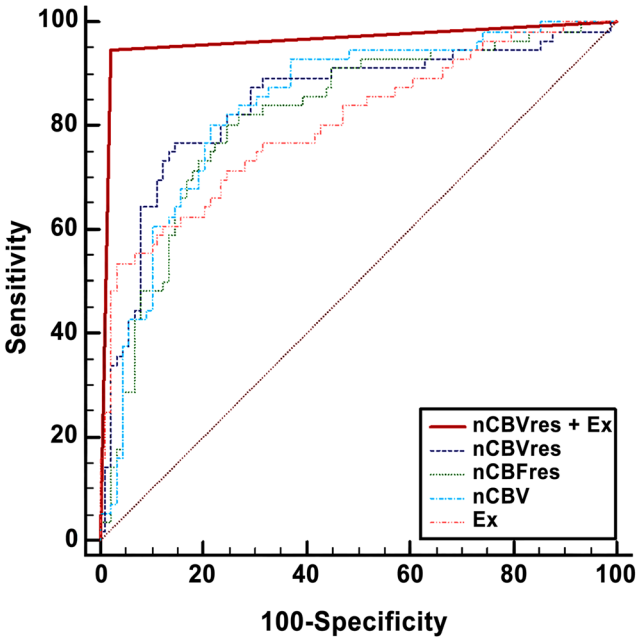

Fig. 4 Receiver operating characteristics curves for perfusion and permeability parameters. Note that the combination of $nCBV_{res}$ and E_x exhibits the highest performance

therefore propose that the standard kinetic model used to estimate CBF from DSC-MRI is extended to also include estimates of permeability and extraction fraction, by modeling the tissue residue function to asymptotically approach a non-zero value reflecting the degree of extravasation.

To reduce the complexity of the model and hence improve stability, a simplified two-compartment model that assumes contrast agent back-flux to be negligible during the observation time was applied. Given the short DSC-MRI imaging time used (less than 2 min), this is thought to be a reasonable assumption. A permeability-related metric, K_2, is also obtained from the Weisskoff-Boxerman leakage method, but this parameter has so far been mainly considered as a by-product of the correction method [24]. Theoretically, the Weisskoff-Boxerman leakage method is inherently sensitive to deviations in MTT in the leaky tissue compared with the MTT of the reference curve. This MTT sensitivity has also been observed in clinical tumor data [25], indicating increased error in K_2 and CBV estimation when tumoral MTT increasingly deviates from that of reference tissue [9]. The residue-based correction method is not sensitive to MTT variations, as MTT is included as a model parameter. However, in the present study, no significant difference in MTT was observed between the glioblastoma and PCNSL groups, and hence, any MTT-induced parameter would be equal in both tumor types when applying the Weisskoff-Boxerman leakage calculation method. The two correction methods were thus found to produce corrected nCBV values with similar diagnostic performance, although the highest single-parameter AUC was obtained from $nCBV_{res}$ derived from the residue-based correction method.

This study has several limitations. First, no direct correlations between DSC parameters and histologic findings such as microvessel density and endothelial markers were performed, but such analyses were beyond the scope of the present work. Second, the permeability-related parameters obtained from DSC-MRI are potentially challenging to interpret because of

Table 4 Effect of adding the permeability parameter to cerebral blood volume from dynamic susceptibility contrast MRI in the differentiation of primary central nervous system lymphoma from glioblastoma

			AUC (95% CI)	Threshold	Sensitivity (%)	Specificity (%)	Cross-validated AUC
Perfusion + permeability parameter	$nCBV_{res} + E_x$	Ref	0.96 (0.92, 0.99)	–	94.6	97.8	0.95
Perfusion parameters	$nCBV_{res}$	< .001	0.84 (0.77, 0.90)	≤ 1.99	76.8	85.4	0.81
	$nCBF_{res}$	< .001	0.82 (0.74, 0.88)	≤ 1.56	80.4	75.3	0.77
	nCBV	< .001	0.84 (0.77, 0.90)	≤ 1.81	78.6	78.7	0.80
Permeability parameters	E_x	< .001	0.80 (0.73, 0.86)	> 9.3	53.6	95.5	0.76

The *p* value refers to the significance of the difference in diagnostic performance between the combined perfusion and permeability parameter and the single parameters of either perfusion or permeability (Bonferroni corrected, $p < 0.0125$). *AUC*, area under the receiver operating characteristics curve; E_x, extraction fraction; *CBV*, cerebral blood volume

a combination of T1- and T2*-dominant leakage relaxation effects once the agent extravasates to the EES. In our study, we used a pre-dose combined with a low flip angle to minimize confounding T1-relaxation effects. Our implementation of the leakage correction methods also enables separation of T1- from T2*-limited leakage effects, by allowing the resulting leakage constants (K_a and K_2) to assume both positive and negative values [9, 25]. We were therefore able to confirm that the overall leakage effect in both tumor types and with both correction methods corresponded to a dominant T2*-based relaxation in the EES. Nonetheless, the resulting dose-response from the leakage fraction of the contrast agent could still be influenced by T1-shortening, introducing errors in the resulting permeability constants. The problem of concomitant T1- and T2*-effects is a fundamental weakness of current DSC-MRI methods, which may be overcome by the introduction of more quantitative approaches like multi-echo acquisitions [26]. Finally, these DSC-MRI-derived metrics should be validated against DCE-MRI-based analyses, and future studies are needed to correlate these parameters, preferably using a dual injection combined DCE- and DSC-MRI protocol.

In conclusion, the combined analysis of E_x and CBV derived from a single DSC-MRI acquisition provided better diagnostic performance in the differentiation of PCNSL from glioblastoma than standard CBV analysis. The combined analysis can be fully automated without the need for manual definition of an AIF or reference tissue and obtained with a single-dose of contrast agent usage, thereby making this approach feasible and attractive in a clinical setting.

Funding This research was supported by the National Research Foundation of Korea (NRF) Grant by the Korean government (MSIP) (grant nos. NRF-2017R1A2A2A05001217 and NRF-2017R1C1B2007258).

Compliance with ethical standards

Guarantor The scientific guarantor of this publication is Ho Sung Kim.

Conflict of interest The authors of this manuscript declare no relationships with any companies, whose products or services may be related to the subject matter of the article.

Statistics and biometry No complex statistical methods were necessary for this paper.

Informed consent Written informed consent was waived by the Institutional Review Board.

Ethical approval Institutional Review Board approval was obtained.

Methodology
- retrospective
- cross-sectional study
- performed at one institution

References

1. Thompson G, Mills S, Coope D, O'connor J, Jackson A (2011) Imaging biomarkers of angiogenesis and the microvascular environment in cerebral tumours. Br J Radiol 84:S127–S144
2. Koeller KK, Smirniotopoulos JG, Jones RV (1997) Primary central nervous system lymphoma: radiologic-pathologic correlation. Radiographics 17:1497–1526
3. Hartmann M, Heiland S, Harting I et al (2003) Distinguishing of primary cerebral lymphoma from high-grade glioma with perfusion-weighted magnetic resonance imaging. Neurosci Lett 338:119–122
4. Liao W, Liu Y, Wang X et al (2009) Differentiation of primary central nervous system lymphoma and high-grade glioma with dynamic susceptibility contrast-enhanced perfusion magnetic resonance imaging. Acta Radiol 50:217–225
5. Xu W, Wang Q, Shao A, Xu B, Zhang J (2017) The performance of MR perfusion-weighted imaging for the differentiation of high-grade glioma from primary central nervous system lymphoma: a systematic review and meta-analysis. PLoS One 12:e0173430
6. Kickingereder P, Sahm F, Wiestler B et al (2014) Evaluation of microvascular permeability with dynamic contrast-enhanced MRI for the differentiation of primary CNS lymphoma and glioblastoma: radiologic-pathologic correlation. AJNR Am J Neuroradiol 35:1503–1508
7. Zhao J, Yang ZY, Luo BN, Yang JY, Chu JP (2015) Quantitative evaluation of diffusion and dynamic contrast-enhanced MR in tumor parenchyma and peritumoral area for distinction of brain tumors. PLoS One 10:e0138573
8. Nguyen TB, Cron GO, Mercier JF et al (2012) Diagnostic accuracy of dynamic contrast-enhanced MR imaging using a phase-derived vascular input function in the preoperative grading of gliomas. Am J Neuroradiol 33:1539–1545
9. Bjornerud A, Sorensen AG, Mouridsen K, Emblem KE (2011) T1- and T2*-dominant extravasation correction in DSC-MRI: part I–theoretical considerations and implications for assessment of tumor hemodynamic properties. J Cereb Blood Flow Metab 31:2041–2053
10. Paulson ES, Schmainda KM (2008) Comparison of dynamic susceptibility-weighted contrast-enhanced MR methods: recommendations for measuring relative cerebral blood volume in brain tumors. Radiology 249:601–613
11. Weisskoff R, Boxerman J, Sorensen A, Kulke S, Campbell T, Rosen B (1994) Simultaneous blood volume and permeability mapping using a single Gd-based contrast injection. Proceedings of the Society of Magnetic Resonance, Second Annual Meeting, San Francisco, Calif. Berkeley, pp p.279
12. Louis DN, Perry A, Reifenberger G et al (2016) The 2016 World Health Organization classification of tumors of the central nervous system: a summary. Acta Neuropathol 131:803–820
13. Bjornerud A, Kleppesto M, Batchelor TT, Wen P, Sorensen AG, Emblem KE (2016) Test-retest stability of MTT insensitive CBV leakage correction in DSC-MRI Proceedings of the 24th Annual Meeting of International Society of Magnetic Resonance in Medicine (ISMRM), Singapore, Singapore
14. Boxerman JL, Schmainda KM, Weisskoff RM (2006) Relative cerebral blood volume maps corrected for contrast agent extravasation significantly correlate with glioma tumor grade, whereas uncorrected maps do not. AJNR Am J Neuroradiol 27:859–867
15. Sourbron S, Ingrisch M, Siefert A, Reiser M, Herrmann K (2009) Quantification of cerebral blood flow, cerebral blood volume, and blood-brain-barrier leakage with DCE-MRI. Magn Reson Med 62:205–217
16. Ostergaard L, Weisskoff RM, Chesler DA, Gyldensted C, Rosen BR (1996) High resolution measurement of cerebral blood flow

using intravascular tracer bolus passages. Part I: mathematical approach and statistical analysis. Magn Reson Med 36:715–725
17. Emblem KE, Bjornerud A (2009) An automatic procedure for normalization of cerebral blood volume maps in dynamic susceptibility contrast-based glioma imaging. AJNR Am J Neuroradiol 30:1929–1932
18. DeLong ER, DeLong DM, Clarke-Pearson DL (1988) Comparing the areas under two or more correlated receiver operating characteristic curves: a nonparametric approach. Biometrics 44:837–845
19. Jain R (2011) Perfusion CT imaging of brain tumors: an overview. AJNR Am J Neuroradiol 32:1570–1577
20. Molnar PP, O'Neill BP, Scheithauer BW, Groothuis DR (1999) The blood-brain barrier in primary CNS lymphomas: ultrastructural evidence of endothelial cell death. Neuro Oncol 1:89–100
21. Larsson HB, Courivaud F, Rostrup E, Hansen AE (2009) Measurement of brain perfusion, blood volume, and blood-brain barrier permeability, using dynamic contrast-enhanced T(1)-weighted MRI at 3 tesla. Magn Reson Med 62:1270–1281
22. Sorensen AG, Batchelor TT, Zhang WT et al (2009) A "vascular normalization index" as potential mechanistic biomarker to predict survival after a single dose of cediranib in recurrent glioblastoma patients. Cancer Res 69:5296–5300
23. Alger JR, Schaewe TJ, Lai TC et al (2009) Contrast agent dose effects in cerebral dynamic susceptibility contrast magnetic resonance perfusion imaging. J Magn Reson Imaging 29:52–64
24. Liu HL, Wu YY, Yang WS, Chen CF, Lim KE, Hsu YY (2011) Is Weisskoff model valid for the correction of contrast agent extravasation with combined T1 and T2* effects in dynamic susceptibility contrast MRI? Med Phys 38:802–809
25. Emblem KE, Bjornerud A, Mouridsen K et al (2011) T_1- and T_2*-dominant extravasation correction in DSC-MRI: Part II— predicting patient outcome after a single dose of cediranib in recurrent glioblastoma patients J Cereb Blood Flow Metab 31:2054–2064
26. Grovik E, Redalen KR, Storas TH et al (2017) Dynamic multi-echo DCE- and DSC-MRI in rectal cancer: Low primary tumor Ktrans and ΔR2* peak are significantly associated with lymph node metastasis. J Magn Reson Imaging 46:194–206